processes

MDPI

Article

Quantitative Fault Diagnosis of Planetary Gearboxes Based on Improved Symbolic Dynamic Entropy

Yanliang Wang [1], Jianguo Meng [1,*], Tongtong Liu [2] and Chao Zhang [2]

[1] School of Mechanical Engineering, Inner Mongolia University of Science and Technology, Baotou 014010, China; liangwy1998@163.com
[2] Inner Mongolia Key Laboratory of Intelligent Diagnosis and Control of Mechatronic System, Baotou 014010, China; liuzhaishi@imust.edu.cn (T.L.); zhanghero@imust.edu.cn (C.Z.)
* Correspondence: mjg101@163.com; Tel.: +86-189-4720-8947

Abstract: To realize a quantitative diagnosis of faults in the planetary gearboxes of wind turbines by processing the complex frequency signals of the planetary gear boxes and avoiding the aliasing problem of the resulting frequencies, this paper proposes a diagnosis method based on improved variational mode decomposition (IVMD) and average multi-scale double symbolic dynamic entropy (AMDSDE). Moreover, an IVMD algorithm based on multi-scale permutation entropy is introduced to reduce noise interference and realize signal demodulation. Considering the effects of complex transfer paths and the correlation between current and adjacent state modes, AMDSDE is proposed. Each fault size is obtained based on the entropy curve, and the AMDSDE of unknown faults is calculated. To verify the accuracy of the proposed method, simulations and experimental signals are processed. The quantitative diagnosis of the planetary gearboxes of wind turbines is realized, providing a reliable basis for evaluating the health status of planetary gearboxes.

Keywords: entropy; fault diagnosis; signal analysis; signal-to-noise ratio; signal processing algorithms

Citation: Wang, Y.; Meng, J.; Liu, T.; Zhang, C. Quantitative Fault Diagnosis of Planetary Gearboxes Based on Improved Symbolic Dynamic Entropy. *Processes* **2024**, *12*, 1415. https://doi.org/10.3390/pr12071415

Academic Editor: Olympia Roeva

Received: 17 May 2024
Revised: 24 June 2024
Accepted: 2 July 2024
Published: 7 July 2024

1. Introduction

With the steady advancement of the 'double carbon' policy in China, the application of wind turbines has gradually become more widespread. As the core components of wind turbines, monitoring the status of planetary gearboxes is crucial to their operating conditions and health. During the operation of planetary gearboxes, various types of faults may occur, such as tooth breakage, tooth loss, cracks, and pitting, while certain faults such as wear can persist throughout their life cycle. Due to the complexity related to the working environment and equipment, the downtime for maintenance of planetary gearboxes can severely affect the overall productive efficiency. So, the quantitative diagnosis of key component faults in planetary gearboxes is of particular importance. As external excitations change, the input speed of the planetary gearbox changes as well, due to which conventional fault [1] frequency feature extraction methods experience a significant "frequency ambiguity" phenomenon. To eliminate this phenomenon, the original signal needs to be resampled in the angle domain and be transformed into an angle-domain stationary signal that is not affected by speed changes. These may result in significant noise interference in the gearbox vibration signal, in addition to fault impact signals. At the same time, the unique multi-point meshing characteristics and signal transmission path differences of planetary gearboxes make the collected vibration signal a complex modulation signal. Consequently, it is difficult to extract quantitative indicators for the modulation signal of planetary gearboxes that contain strong noise interference. In this case, the signal needs to be demodulated and denoised before calculating its quantitative indicators.

To this end, Huang et al. [2] proposed a new algorithm called tensor singular spectral decomposition for adaptively decomposing multi-channel time series. In recent years, with the intersection of fault diagnosis and computer fields, fault diagnosis methods [3–5]

based on deep learning have gradually become popular, such as transfer learning, digital twins, etc. In Ref. [6], a coupled convolutional residual network is proposed to realize the information stream fusion. To improve diagnostic accuracy, Zhang et al. [7] proposed a digital twin-driven fault diagnosis framework using labeled simulated data and unlabeled measured data to achieve cross-domain feature alignments in scenarios where the health conditions of the measured data are unknown. Ref. [8] innovatively proposed a universal source-free domain adaptation method that can handle cross-domain fault diagnosis scenarios without access to source data and is free of explicit assumptions about target fault modes.

Their method can better extract weak fault quantification features hidden in the original multi-channel signal. Variational modal decomposition (VMD) was first proposed by Dragomiretskiy et al. [9] and is an algorithm that can effectively demodulate multiple impact signals with a good denoising effect. VMD uses the non-recursive decomposition method that can effectively solve the endpoint effects and mode-mixing problems of empirical modal decomposition (EMD) and local mean decomposition (LMD). Currently, a large body of research has demonstrated that VMD is effective and has significant advantages in signal demodulation and denoising [10–13]. Li et al. [14] proposed a fault diagnosis method for gear cracks and broken teeth based on variational modal decomposition–data-driven time—frequency analysis (VMD–DDTFA), and] reported that the VMD algorithm has a certain effect on signal denoising. Zheng et al. [15] introduced a locust optimization algorithm with correlation kurtosis as the adaptive fitness function, which can adaptively select the VMD parameters. Tang et al. [16] proposed fault identification methods for key parts of internal combustion engines based on VMD. Li et al. [17] proposed an optimization algorithm for VMD transformation parameters, which is conducive to signal decomposition and reconstruction, and applied it to bearing fault discrimination. The accuracy of obtaining the intrinsic mode function (IMF) components via VMD transformation mainly depends on the selection of parameters. The currently available research mainly selects parameters based on prior knowledge or optimizes only one of the parameters, limiting the applicability of the method. Aiming at the shortcomings of the traditional VMD algorithm, this paper proposes an improved VMD (IVMD) algorithm based on multi-scale permutation entropy (MPE), which can select the optimal combination of VMD parameters to obtain the intrinsic modal components containing fault signals.

It is of great significance to introduce a feature indicator that can reflect the size of the fault for the diagnosis of key planetary gearbox components. Studies have revealed that entropy has the characteristic of effectively reflecting changes in fault size. The entropy theory was first proposed by Shannon [18]. Shannon entropy paved the way for the further study and application of the entropy theory. Khandaker [19] proposed a scale-independent flexible bearing health monitoring index based on the energy entropy of the time–frequency manifold, which combined the concepts of the time–frequency manifold and Shannon entropy to construct an accurate bearing health monitoring index, and several applications in the field of fault diagnosis have been reported [20–22]. Bhabesh proposed an improved distribution entropy (ImDistEn) in Ref. [23], which achieved a clear distinction between different classes of real-world signals, in addition to accurately evaluating the complexity of various synthetic signals. The above method is applied to the analysis of complex signals; however, there are still certain limitations. Daw et al. [24] proposed a symbolic time series analysis algorithm based on the theories of symbolic dynamics, chaotic time series analysis, and information theory, which is faster, simpler, and more effective in processing vibration signals compared to other entropy-based methods. In particular, the algorithm converts the original time series into a symbolic sequence with a finite number of values, which is a coarse-grained process. Based on symbolic time series analysis, Kurths et al. [25] proposed the concept of symbolic dynamic entropy (SDE). In another study, Chen et al. [26] applied SDE to bearing fault diagnosis. Nonetheless, existing SDE algorithms consider only the effect of the probability of each state mode during their calculation process, and

they perform well in processing simple signals such as bearing faults or gear faults of fixed-shaft gearboxes.

Due to the modulation phenomenon and phase difference caused by the transmission path in planetary gearboxes, traditional SDE algorithms cannot contain all the fault information, leading to an inaccurate reflection of the actual fault condition of the planetary gearbox.

The signals of planetary gearboxes are complex, and the symbolic entropy of a single scale is inadequate for extracting the true features of the signal. To address this issue, Costa et al. [27] introduced a scale factor and proposed the multi-scale entropy (MSE) concept. Ding et al. [28] introduced SDE Multi-scale to endow the extracted features with greater advantages and higher sensitivity. Li et al. [29] proposed the multi-scale symbolic dynamic entropy (MSDE) method and applied it to extract the fault features of a planetary gearbox, achieving good results. In their work, Han et al. [30] applied MSDE to fault diagnosis of bearings and identified the fault type and degree of rolling bearings.

Currently, the scale selection of multi-scale entropy relies primarily on experience. A scale that is too small may lead to signal aliasing, while a scale that is too large may result in scale repetition and computational efficiency reduction. Hence, the suitability of the selected scale directly affects the authenticity of the entropy value in reflecting signal features. Furthermore, due to the complex operating conditions of such equipment, various noise impacts may appear in the time domain signal, causing the entropy values to jump and affecting the accuracy. To address the problems of the above research, where traditional SDE algorithms cannot fully capture all the fault information of planetary gearboxes, this paper takes the relationship between the state mode matrix and its adjacent mode matrix into consideration and introduces the concept of double symbolic dynamic entropy (DSDE). To address the issues relating to scale selection and entropy parameter selection, this paper builds on the DSDE concept and proposes AMDSDE. This algorithm scales the DSDE and calculates the average of the resulting entropy values to avoid the effects of individual noise shocks on the overall system. In addition, it adaptively selects the best scale based on the entropy value change characteristics at each scale. The 3-sigma principle is applied to calculate the failure threshold for fault scales. Subsequently, the proposed method is used to process simulated and experimental signals of various sizes of sun gear faults in planetary gearboxes.

The remainder of this paper is as follows. Section 2 presents the basic theory and parameter optimization selection method of the traditional VMD algorithm. Section 3 introduces the calculation method of the SDE and the AMDSDE theory. Section 4 demonstrates the application of the IVMD and AMDSDE methods in the analysis of planetary gearbox fault signals and the calculation of critical thresholds using the 3-sigma principle under actual working conditions. Lastly, Section 5 draws the conclusions.

2. IVMD Algorithm

VMD is mainly used for constrained variational problems to achieve an adaptive solution, obtaining the central frequency and bandwidth of each component through iterative calculations, and ultimately dividing the original signal into several IMF signals in the frequency domain.

The parameters of the VMD algorithm include the number of decomposition layers K, the Lagrange multiplier λ, the quadratic penalty factor α, the fidelity parameter τ, the initial center frequency $\hat{\omega}_k^1$, and the convergence condition parameter ε. Among them, according to Ref. [9], K, α, and τ are the parameters that significantly affect the VMD algorithm, and selecting different values would result in different decomposition results. More specifically, K determines the number of IMF components; thus, it affects the actual number of resonance frequency bands contained in the IMF components. The quadratic penalty factor α affects the optimization bandwidth range of the IMF components and directly affects their convergence capability. Moreover, the selection of the fidelity parameter τ directly affects the energy loss ratio between the sum of all IMF components and the original signal. Currently, the research on the input variable parameters relies mainly on empirical values

or focuses only on the number of decomposition layers K. The VMD transformation of each parameter is a combination factor with cross-effects; by simply considering the variation of a single parameter, accurate IMF components cannot be obtained. Therefore, it is essential to select a more targeted parameter combination based on the signal characteristics.

This study found that the permutation entropy can reflect the periodicity of vibration signals. The purpose of VMD transformation is to obtain a series of impact signals with different frequencies exhibiting periodic characteristics. Consequently, this paper proposes an IVMD algorithm based on multi-scale permutation entropy. In particular, based on the principle of the minimum permutation entropy of IMF components, the grid search algorithm is employed to optimize the VMD parameters. The specific steps for parameter optimization are as follows:

(1) The search range, search step, initial value of the decomposition layer K, and the quadratic penalty factor α are set.
(2) A two-dimensional grid is constructed on the coordinate system (K, α), the grid is divided according to the search range and search step, and the VMD corresponding to each grid point parameter is calculated.
(3) Based on the parameter combination corresponding to each grid point, the signal of each fault size of the planetary gearbox (Figure 1) sun gear is decomposed via VMD, and the mean multi-scale permutation entropy value of all IMF components is calculated separately.
(4) The mean multi-scale permutation entropy value of all grid points is calculated in turn. The grid (K, α) corresponding to the maximum entropy value is the optimal decomposition parameter combination.
(5) The (K, α) obtained in Step 4 is set as the combination parameter of VMD transformation, VMD transformation on the signal is performed, and the spectrum of the reconstructed signal is calculated to determine the fault type.

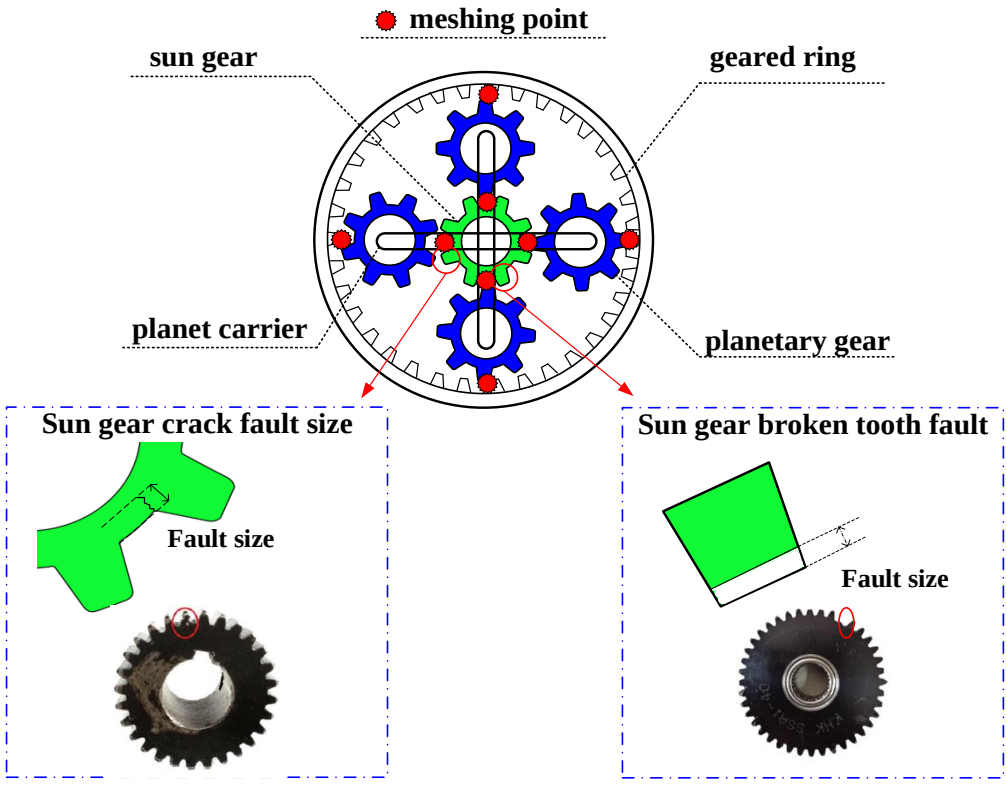

Figure 1. Planetary gear structure diagram and fault diagram.

To verify the effectiveness of the proposed IVMD algorithm, this paper processed simulated sun gear fault signals of a planetary gearbox using both the traditional VMD

and IVMD algorithms. To maintain generality, Gaussian white noise with a SNR of 15 was added to the simulated fault signals. Figure 2 exhibits the results of the traditional VMD algorithm. Figure 3 demonstrates the results of the IVMD algorithm.

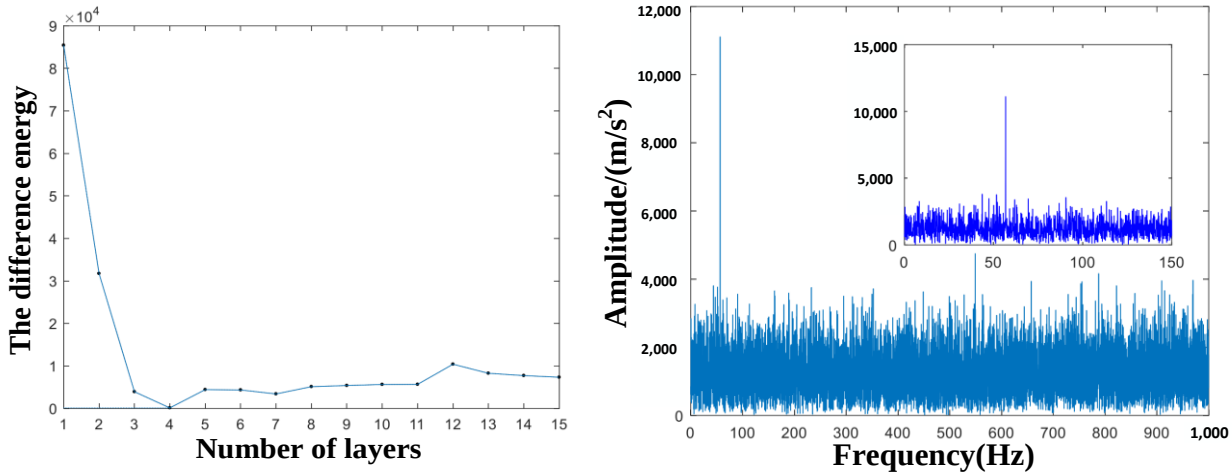

(**a**) (**b**)

Figure 2. Traditional VMD algorithm results for a sun gear fault simulation signal. (**a**) Plot of selecting the optimal decomposition layer. (**b**) Spectrum analysis of the reconstructed signal after VMD.

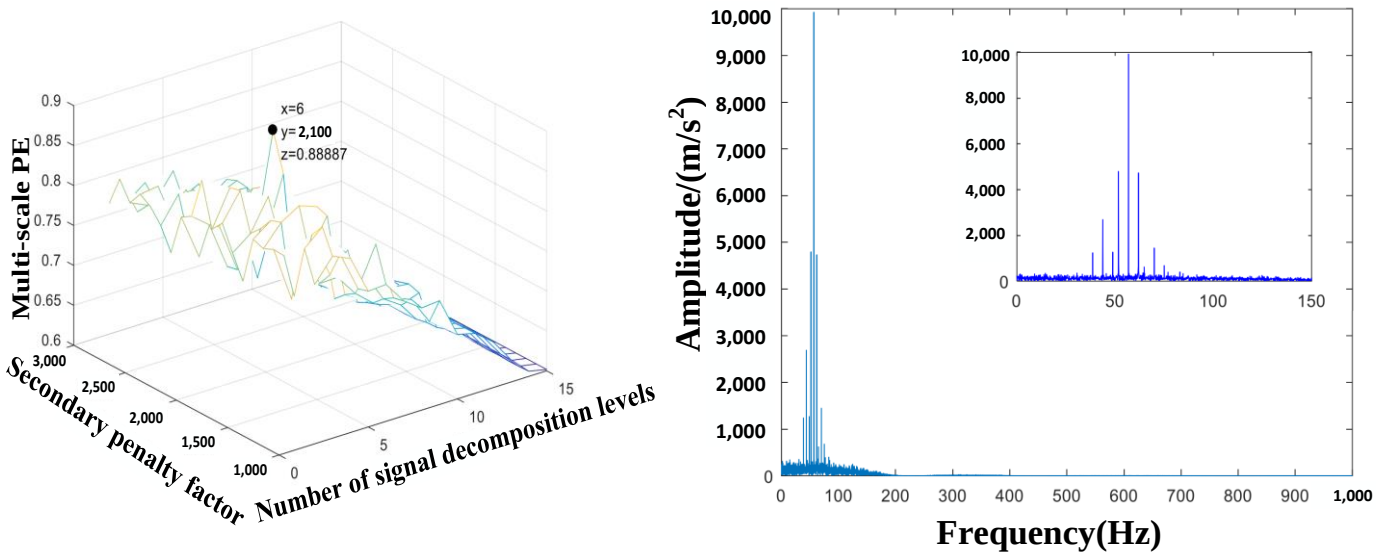

(**a**) (**b**)

Figure 3. IVMD algorithm results for a sun gear fault simulation signal. (**a**) The optimal parameters for the sun gear fault. (**b**) Spectrum analysis of the reconstructed signal.

To verify the effectiveness of the improved VMD algorithm, this paper used the traditional VMD algorithm and the improved VMD algorithm to process the planetary gearbox sun gear fault simulation signal. Without losing generality, this paper added Gaussian white noise with a signal–noise intensity of 15 to the simulated fault signal. Figure 1 shows the results of the traditional VMD algorithm. In particular, Figure 1a presents the optimal decomposition level, which was determined to be k = 4. Figure 1b displays the reconstructed signal spectrum after VMD processing, which displays the fault frequency; however, it was heavily distorted by noise with the fault harmonic frequencies being submerged in the noise. According to Figure 3a, the optimal VMD parameter combination was k = 6 and α = 2100. Figure 3b demonstrates that the noise was effectively suppressed

by the improved algorithm, and the fault frequency and its harmonic frequencies were obtained accurately. Overall, the comparison of the results of the two methods confirms the superiority of the proposed algorithm and validates its effectiveness.

3. Symbolic Dynamic Entropy Optimization Algorithm

3.1. Basic Calculation Principles of Traditional SDE

3.1.1. SDE

Assuming that the time domain signal sequence $\{Z\} = \{z1, z2, z3, \ldots, zN\}$ is a vibration signal of a faulty planetary gearbox with a length of N, the main parameters involved in the calculation of the symbolic dynamic information entropy of the signal are the symbol number s, the embedding dimension m, and the time delay parameter λ. The calculation process includes the following three steps:

(1) Symbolization of time domain signals. The amplitude of the time domain signal is divided into $\boldsymbol{S}$ intervals according to the principle of average amplitude division, and the corresponding amplitude intervals are shown in (1).

$$\left\{ \begin{array}{c} \left(\boldsymbol{A_{min}}, \boldsymbol{A_{min}} + \frac{\boldsymbol{1}}{\boldsymbol{s}}(\boldsymbol{A_{max}} - \boldsymbol{A_{min}})\right), \\ \left[\boldsymbol{A_{min}} + \frac{\boldsymbol{1}}{\boldsymbol{s}}(\boldsymbol{A_{max}} - \boldsymbol{A_{min}}), \boldsymbol{A_{min}} + \frac{\boldsymbol{2}}{\boldsymbol{s}}(\boldsymbol{A_{max}} - \boldsymbol{A_{min}})\right. \\ \cdots \\ \left.\left[\boldsymbol{A_{min}} + \frac{\boldsymbol{s-1}}{\boldsymbol{s}}(\boldsymbol{A_{max}} - \boldsymbol{A_{min}}), \boldsymbol{A_{min}} + \frac{\boldsymbol{s}}{\boldsymbol{s}}(\boldsymbol{A_{max}} - \boldsymbol{A_{min}})\right]\right] \end{array} \right\} \tag{1}$$

Assuming that the symbol values corresponding to each interval are $\sigma_i (i = 1, 2, \ldots, s)$, for different time domain signals within each interval, the corresponding symbol values are selected and assigned to the original time domain amplitudes to obtain the corresponding symbol sequence. Thus, the newly obtained symbol sequence is:

$$\boldsymbol{Y}\{\boldsymbol{y_n}(\boldsymbol{k}), \boldsymbol{n} = \boldsymbol{1}, \boldsymbol{2}, \ldots, \boldsymbol{N}, \boldsymbol{k} = \boldsymbol{1}, \boldsymbol{2}, \ldots \boldsymbol{s}\} \tag{2}$$

where, $y_n(k)$ represents the symbol corresponding to the nth point of the original time domain signal.

(2) Construction of a state pattern matrix and calculation of the state pattern probability. According to the previously set embedding dimension m and time delay parameter λ, the symbol sequence is divided into $N - (m-1)\lambda$ sub-vectors $\boldsymbol{Y_i^{m,\lambda}}\{\boldsymbol{y}(\boldsymbol{i}), \boldsymbol{y}(\boldsymbol{i}+\boldsymbol{\lambda}), \ldots, \boldsymbol{y}(\boldsymbol{i}+(\boldsymbol{m}-\boldsymbol{1})\boldsymbol{\lambda})\}$ in turn, which are constructed into a state pattern matrix $\boldsymbol{Y_i^{m,\lambda}}$, as shown in (3):

$$\boldsymbol{Y_i^{m,\lambda}} = \begin{bmatrix} \boldsymbol{y_1}(\boldsymbol{k}) & \boldsymbol{y_1}(\boldsymbol{k}) & \cdots & \boldsymbol{y_{1+(m-1)\lambda}}(\boldsymbol{k}) \\ \boldsymbol{y_1}(\boldsymbol{k}) & \boldsymbol{y_1}(\boldsymbol{k}) & \cdots & \boldsymbol{y_{2+(m-1)\lambda}}(\boldsymbol{k}) \\ \vdots & \vdots & \vdots & \vdots \\ \boldsymbol{y_{N-(m+1)\lambda}}(\boldsymbol{k}) & \boldsymbol{y_{N-M\lambda}}(\boldsymbol{k}) & \cdots & \boldsymbol{y_N}(\boldsymbol{k}) \end{bmatrix} k \in [1, 2, \ldots, s] \tag{3}$$

In theory, with S symbol numbers and the set embedding dimension m, there are s^m potential symbol arrangement state patterns. Based on the parameters set in SDE, it can be derived from (3) that $\boldsymbol{N} - (\boldsymbol{m}-\boldsymbol{1})\boldsymbol{\lambda}$ permutation state patterns appear in the obtained state pattern matrix. The number of times each permutation state pattern $q_a^{s,m,\lambda}$ appears is counted and its probability, denoted as $pq_a^{s,m,\lambda}$, is calculated as follows:

$$\boldsymbol{P}\left(\boldsymbol{q_a^{s,m,\lambda}}\right) = \frac{\left\| \left\{ \boldsymbol{i} : \boldsymbol{i} \le \boldsymbol{N} - (\boldsymbol{m}-\boldsymbol{1})\boldsymbol{\lambda}, \boldsymbol{type}\left(\boldsymbol{Y_i^{m,\lambda}}\right) = \boldsymbol{q_a^{s,m,\lambda}} \right\} \right\|}{\boldsymbol{N} - (\boldsymbol{m}-\boldsymbol{1})\boldsymbol{\lambda}} \tag{4}$$

where $type(\cdot)$ represents the mapping relationship from the symbol sequence to the state pattern matrix and $\|\cdot\|$ represents the norm of the set. The state pattern probability of each permutation state pattern is calculated and all state pattern probabilities are combined

into a state pattern probability matrix $\boldsymbol{P}\left(q_1^{s,m,\lambda}\right), \boldsymbol{P}\left(q_2^{s,m,\lambda}\right), \ldots, \boldsymbol{P}\left(q_{s^m}^{s,m,\lambda}\right)$. From the fact that the state pattern includes all possibilities, it can be known that the sum of all state pattern probabilities is 1, $\boldsymbol{sum}\left(\boldsymbol{P}\left(q_a^{s,m,\lambda}\right)\right)$, and the accuracy of the calculation process can be calibrated.

(3) The SDE is calculated and normalized. According to the Shannon entropy definition in information theory, SDE is defined as the cumulative value of the product of the probability of each state mode and its logarithm. Since the probability values of the state mode are all decimal values between 0 and 1, the logarithmic values are all negative, so the negation of the SDE value is finally taken, as shown in (5).

$$\boldsymbol{SDE}(\boldsymbol{Z}, \boldsymbol{s}, \boldsymbol{m}, \boldsymbol{\lambda}) = -\sum_{\boldsymbol{a}=\boldsymbol{1}}^{\boldsymbol{s^m}} \boldsymbol{P}(q_a^{s,m,\lambda}) \boldsymbol{log}(\boldsymbol{P} q_a^{s,m,\lambda}) \tag{5}$$

According to (4), when all state pattern probabilities are equal, i.e., $P\left(q_a^{s,m,\lambda}\right) = 1/s^m$, the maximum SDE value is obtained, as shown in (6).

$$\boldsymbol{SDE}(\boldsymbol{Z}, \boldsymbol{s}, \boldsymbol{m}, \boldsymbol{\lambda})_{\boldsymbol{max}} = -\sum_{\boldsymbol{a}=\boldsymbol{1}}^{\boldsymbol{s^m}} \left(\frac{\boldsymbol{1}}{\boldsymbol{s^m}} \boldsymbol{log}\left(\frac{\boldsymbol{1}}{\boldsymbol{s^m}} \right) \right) = -\boldsymbol{log}\left(\frac{\boldsymbol{1}}{\boldsymbol{s^m}} \right) = \boldsymbol{log}(\boldsymbol{s^m}) \tag{6}$$

SDE is normalized based on (5) and (6), as described by (7).

$$\boldsymbol{SDE}(\boldsymbol{Z}, \boldsymbol{s}, \boldsymbol{m}, \boldsymbol{\lambda}) = \frac{\boldsymbol{SDE}(\boldsymbol{Z}, \boldsymbol{s}, \boldsymbol{m}, \boldsymbol{\lambda})}{\boldsymbol{log}(\boldsymbol{s^m})} \tag{7}$$

3.1.2. MSDE

The concept of multi-scale analysis was first proposed by Costa [24] with the main purpose of measuring the dynamic characteristics of time series at different scales. Based on the numerous advantages of multi-scale analysis in dealing with complex signals, several scholars have conducted a series of studies on MSDE and applied it to the diagnosis of rotating equipment faults, reporting good results. The MSDE calculation process consists mainly of the following two steps:

(1) Coarse-grained segmentation of the original time domain signal. Taking the time domain signal $\{\boldsymbol{Z_i}\} = \{\boldsymbol{z_1}, \boldsymbol{z_2}, \boldsymbol{z_3} \ldots, \boldsymbol{z_N}\}$ with length N of the gear teeth with missing tooth fault as the research object, the time domain signal is scaled by coarse-grained segmentation. Assuming that the scaling factor is τ, various scale time domain sequences $\boldsymbol{y} = \left\{ \boldsymbol{y_j^\tau} \right\}$ are obtained, whose expression is:

$$\boldsymbol{y_j^\tau} = \frac{\boldsymbol{1}}{\boldsymbol{\tau}} \sum_{\boldsymbol{i}=\boldsymbol{j}}^{\boldsymbol{j}+\boldsymbol{\tau}-\boldsymbol{1}} \boldsymbol{z_i} \quad \boldsymbol{1} \le \boldsymbol{j} \le \boldsymbol{N} - \boldsymbol{\tau} + \boldsymbol{1} \tag{8}$$

The scaling factor $\boldsymbol{\tau}$ is adjusted to obtain time series at different scales. Clearly, when $\boldsymbol{\tau}$ = 1, the obtained time series is a single-scale time series, and the calculation result is equivalent to directly calculating the SDE value of the signal.

(2) The SDE of time series $\left\{ \boldsymbol{y_j^\tau} \right\}$ at different scales was calculated.

$$\boldsymbol{MSDE}(\boldsymbol{Z}, \boldsymbol{S}, \boldsymbol{m}, \boldsymbol{\lambda}, \boldsymbol{\tau}) = \boldsymbol{SDE}(\boldsymbol{Y_j^\tau}, \boldsymbol{s}, \boldsymbol{m}, \boldsymbol{\lambda}) \tag{9}$$

3.2. Improved AMDSDE

3.2.1. AMDSDE

The symbol sequence consists of a series of pattern intervals of continuous arrangement states. Due to the complex composition characteristics of the planetary gear signal of a wind turbine, the fault frequency information is contained in different pattern intervals. The traditional symbolic dynamic information entropy only considers the entropy value

changes in each state mode, but it does not consider the correlation between different state modes and cannot include all fault information. If the parameters are adjusted to ensure that a single pattern interval contains all fault information, the calculated MSDE will deviate greatly from its true result. To address this problem, this paper proposes the concept of AMDSDE, which ensures that the parameters of the original state pattern matrix are optimal while containing as much fault information as possible of the planetary gear signals with different amplitudes and phases.

The transmission path of the fault excitation source signal from the planetary gearbox to the receiving terminal leads to the composition of impact signals with multiple sets of phase and amplitude differences, but with little overall difference; hence, the fault information is mainly contained in a certain state pattern matrix and the adjacent two state pattern matrices. The adjacent pattern of the current state pattern matrix is defined as the state-transition matrix. Based on the state pattern matrix, the pre-transition and post-transition probabilities of the transfer matrix are derived, i.e., $\boldsymbol{P_{pre}}\left(\sigma_b|q_a^{s,m,\lambda}\right)$ *and* $\boldsymbol{P_{post}}\left(\sigma_c|q_a^{s,m,\lambda}\right)$ corresponding to the state transition matrix corresponding to the state pattern matrix is derived as shown in (10) and (11):

$$\boldsymbol{P}\left(\sigma_b\left|q_a^{s,m,\lambda}\right.\right)_{pre} = \boldsymbol{P}\left\{z(j-m\lambda) = \sigma_b|(j-m\lambda) : j, type\left(Z_j^{s,m,\lambda}\right) = q_a^{s,m,\lambda}\right\} \tag{10}$$

$$\boldsymbol{P}\left\{type\left(Z_j^{s,m,\lambda}\right) = q_a^{s,m,\lambda}, z(j-m\lambda) = (\sigma_b|j : j \le N-m\lambda)\right\} \tag{11}$$

Based on the acquired pre/post-transition probability values and according to the definition of SDE (5), the corresponding pre/post-transition SDE calculation equations are derived ((12) and (13)), denoted as $\boldsymbol{SDE_{pre}}$ and $\boldsymbol{SDE_{post}}$, respectively.

$$\boldsymbol{SDE}(Z,s,m,\lambda)_{pre} = -\sum_{a=1}^{s^m}\sum_{b=1}^{s} P\left(q_a^{s,m,\lambda}\right)P\left(\sigma_b\left|q_a^{s,m,\lambda}\right.\right) \tag{12}$$

$$\boldsymbol{SDE}(Z,s,m,\lambda)_{post} = -\sum_{a=1}^{s^m}\sum_{c=1}^{s} P\left(q_a^{s,m,\lambda}\right)P\left(\sigma_c\left|q_a^{s,m,\lambda}\right.\right) \tag{13}$$

Considering the effect of each state probability on the result, the corresponding weight coefficients are added, and the final DSDE is obtained as:

$$\begin{aligned} &\boldsymbol{double}_{SDE(Z,s,m,\lambda)} \\ &\quad = \varphi_1 \cdot \boldsymbol{SDE}(Z,s,m,\lambda)_{pre} + \varphi_2 \cdot \boldsymbol{SDE}(Z,s,m,\lambda)_{pre} \\ &\quad + \varphi_3 \boldsymbol{SDE}(Z,s,m,\lambda)_{pre} \end{aligned} \tag{14}$$

where $\varphi_1, \varphi_2, \varphi_3$ are the weight coefficients that satisfy $\varphi_1 + \varphi_2 + \varphi_3 = 1$.

Similarly, the DSDE is normalized, and it reaches its maximum value only when all the probabilities for state patterns and pre/post-transitions are equal.

$$\begin{aligned} &\left(P\left(q_a^{s,m,\lambda}\right) = \frac{1}{s^m},\right), \left(P\left(q_a^{s,m,\lambda}\right) = \frac{1}{s^m}, P_{pre}\left(\sigma_b\left|q_a^{s,m,\lambda}\right.\right) = \frac{1}{s}, P_{post}\left(\sigma_c\left|q_a^{s,m,\lambda}\right.\right) = \frac{1}{s}\right) \\ &\boldsymbol{double\_SDE}(Z,s,m,\lambda)_{max} \\ &\quad = -\sum_{a=1}^{s^m}\left(\frac{1}{s^m}log\left(\frac{1}{s^m}\right)\right) - \sum_{b=1}^{s}\left(\frac{1}{s}log\left(\frac{1}{s}\right)\right) - \sum_{c=1}^{s}\left(\frac{1}{s}log\left(\frac{1}{s}\right)\right) \\ &\quad = -log\left(\frac{1}{s^m}\right) - log\left(\frac{1}{s}\right) - log\left(\frac{1}{s}\right) = log(s^{m+2}) \end{aligned} \tag{15}$$

Based on (15), $\boldsymbol{double\_SDE}(Z,s,m,\lambda)$ is normalized as described by (16).

$$\boldsymbol{double\_SDE}(Z,s,m,\lambda) = \frac{\boldsymbol{double\_SDE}(Z,s,m,\lambda)}{log(s^{m+2})} \tag{16}$$

For MSDE, the entropy values for each group of fault signals are represented as vectors made up of multiple data groups. To address the issue of misjudgment caused by signal randomness, the mean of all entropy values is calculated. This approach effectively mitigates the problem. Therefore, this paper calculates the mean of the obtained multi-scale DSDE values to derive parameter indicators that can accurately reflect the fault size. Additionally, it performs linear fitting on the entropy values corresponding to each size to produce a quantitative diagnosis curve for the key components of the planetary gearbox.

The main steps of AMDSDE are as follows:

(1) The original time domain signal is segmented into coarse-grained intervals.

(2) The MSDE is computed for all time domain signals $\left\{y_j^\tau\right\}$ at each scale after coarse-graining.

$$\boldsymbol{MSDE}(Y_j^\tau, s, m, \lambda, \tau) = \boldsymbol{SDE}(Y_{js}^\tau, s, m, \lambda) \tag{17}$$

(3) The mean value of the entropy for each scale of the individual MSDE values is computed.

$$\boldsymbol{DSDE}(Z, s, m, \lambda, \tau)_i = \frac{1}{s}\sum_{i=1}^{s} \boldsymbol{MSDE}(Y_j^\tau, s, m, \lambda, \tau) \tag{18}$$

(4) The DSDE is computed at each scale to obtain the AMDSDE.

$$\boldsymbol{AMDSDE}(Z, s, m, \lambda, \tau) = \{\boldsymbol{DSDE}(Z, s, m, \lambda, \tau)_i, i = 1, 2 \ldots, \tau\} \tag{19}$$

To validate the effectiveness of the AMDSDE method, we calculated the AMDSDE for the healthy state of the sun gear in a planetary gearbox, as well as for fault signals with sizes of 0.3 cm, 0.4 cm, 0.5 cm, and 0.6 cm. The entropy curves for each state are shown in Figure 4. We also computed the mean entropy value for each scale and linearized the entropy values for each fault size, as illustrated in Figure 5.

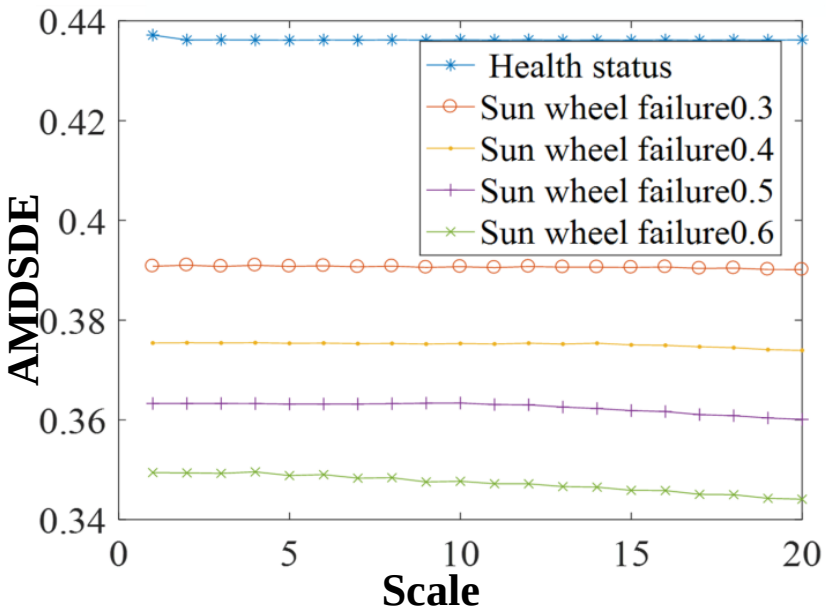

Figure 4. Comparison of AMDSDE curves of sun gear under different fault sizes and health state.

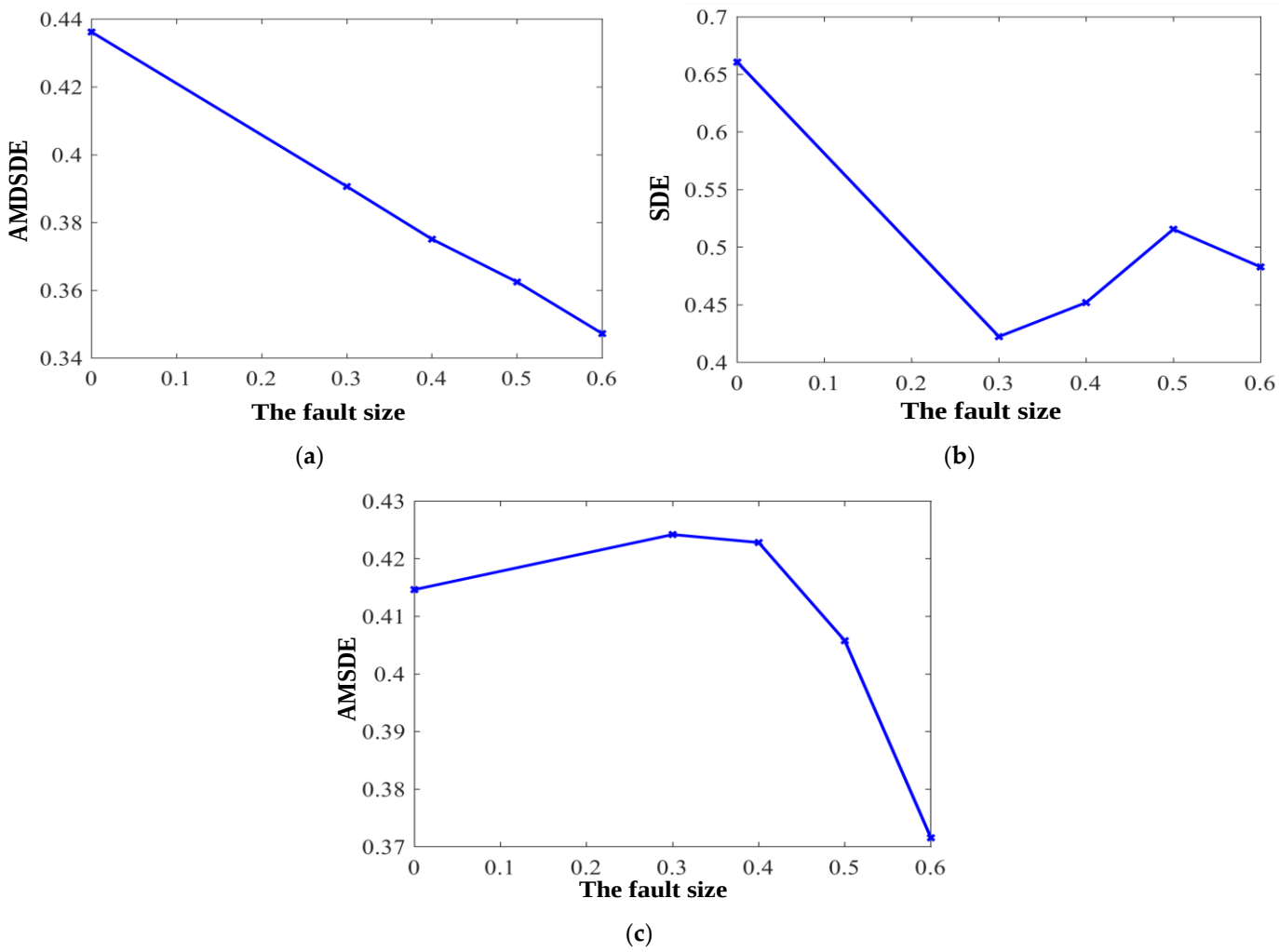

Figure 5. Entropy value curves of sun gear failure in planetary gearbox. (**a**) Planetary gearbox failure AMDSDE curve. (**b**) Planetary gearbox failure SDE curve. (**c**) Planetary gearbox failure AMSDE curve.

Compared to traditional methods, the proposed AMDSDE indicator shows a linear relationship with the fault size of the planetary gearbox. This observation verifies the effectiveness of the method proposed in this study.

3.2.2. AMDSDE Parameter Selection

When applying AMDSDE to extract fault features from planetary gearbox vibration signals, the key parameters are the symbol number s, the embedding dimension m, the time delay λ, and the scale factor τ. Multiple regression analysis was used to investigate the effect of each parameter on AMDSDE, and the results are shown in Table 1 and Figure 6. Ultimately, the parameters were set as follows: s = 8, m = 3, λ = 1, and τ = 20.

Table 1. Effect of multiple regression analysis parameters on AMDSDE index.

Serial Number	Fixed Variable	Independent Variable	AMDSDE
1	s = 8, τ = 20, λ = 1	m∈[1,6]	Figure 5a
2	m = 3, τ = 20, λ = 1	s∈[2,10]	Figure 5b
3	m = 3, τ = 20, s = 8	λ∈[1,5]	Figure 5c

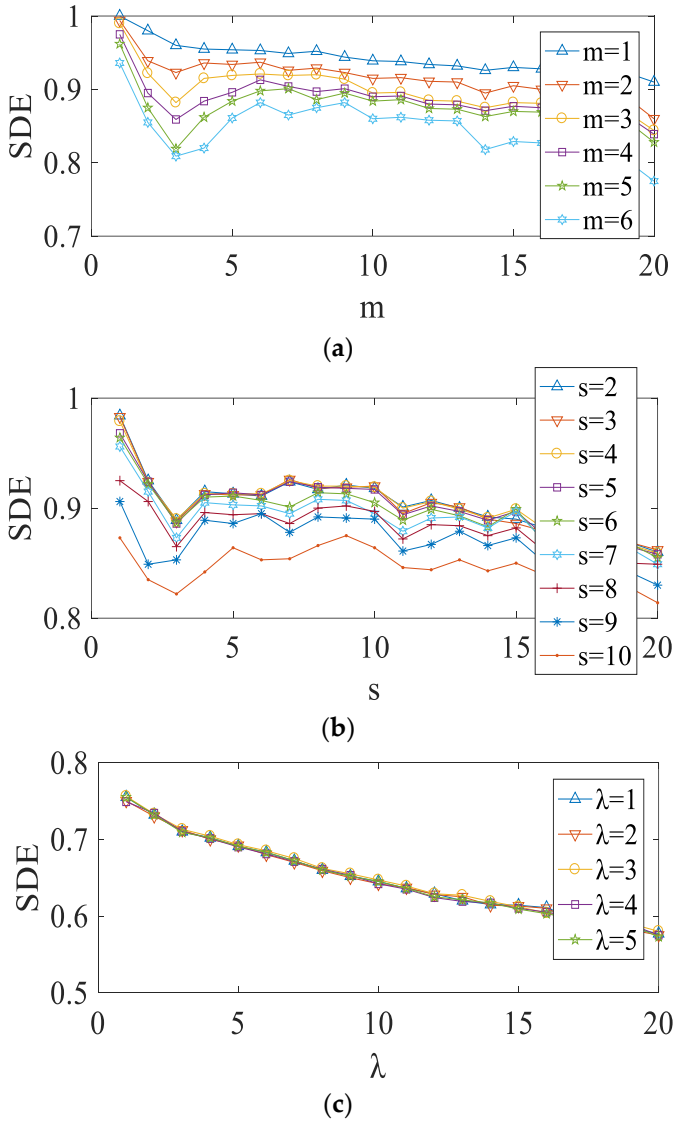

Figure 6. Effect of multiple regression analysis parameters on AMDSDE index. (**a**) Effect of m on SDE. (**b**) Effect of s on SDE. (**c**) Effect of λ on SDE.

3.2.3. Fault Failure Threshold

Currently, the industry lacks a clearly defined range for determining the failure size threshold of planetary gearboxes. Additionally, the judgment criteria vary for different operating conditions. This means that failure assessments are primarily based on empirical judgments, leading to significant uncertainty and potential safety hazards in equipment condition monitoring. In the field of life prediction, the 3-sigma principle is commonly used to calculate the failure threshold for determining component failure.

Assuming that the healthy status vibration time domain signal of the planetary gearbox is $f_h(x) = \{x_1, x_2, \cdots x_N\}$, the mean μ and standard deviation can be separately calculated via (20) and (21), respectively.

$$\mu = \frac{x_1 + x_2 + \ldots x_N}{N} = \frac{\sum_{i=1}^{N} x_i}{N} \tag{20}$$

$$\sigma = \sqrt{\frac{\sum_{i=1}^{N}\left[(x_1 - \mu)^2 + (x_2 - \mu)^2 + \ldots + (x_N - \mu)^2\right]}{N}} \tag{21}$$

According to the 3-sigma principle, the threshold setting range is $[\mu - 3\sigma, \mu + 3\sigma]$. The vibration signal corresponding to the fault size is selected in such a way that its peak envelope line coincides with the threshold curve. In addition, the fault size is set as the failure threshold for the gear of the planetary gearbox. To bring the method closer to practical application, it is necessary to study the condition monitoring between the healthy and failure states of the equipment.

Due to the complex structure of planetary gearboxes, when a gear fails, the fault generates an impact signal transmitted to the sensor as a pulse attenuation signal. The peak-to-peak value of this fault pulse can reflect the fault characteristics. Therefore, considering the fault signal characteristics of a planetary gearbox, it is necessary to obtain its peak-to-peak value, which will be used to calculate the failure threshold. Based on a specific sampling signal, the number of points to be analyzed is calculated using the following equation:

$$N_s = \frac{1}{10} fs * v_s / 60 z_s * t \tag{22}$$

where, N_s is the number of points to be analyzed, f_s is the sampling frequency of the vibration signal, v_s is the input shaft speed of the planetary gearbox, z_s is the number of teeth on the sun gear, and t is the total sampling time.

Figure 7 exhibits the failure threshold curve calculated by the healthy status signal and the 3-sigma principle. The blue curve is the healthy status signal, the red one is the fault signal when the fault size was 3 mm, and the two green dashed lines denote the failure thresholds calculated according to the 3-sigma principle. It can be observed that when the fault size was 3 mm, the vibration amplitude was close to the threshold; thus, the failure size was determined as 3 mm. When the critical components of a gearbox exceed the failure threshold, this poses a serious threat to the safety of the equipment; thus, the faulty component must be replaced. Condition monitoring of the critical components in a planetary gearbox from the onset of weak faults to reaching the failure threshold is of particular importance. The signal entropy values of known fault sizes before the sun gear fails are separately calculated and the fault size–entropy curve is fitted. The fault size of an unknown fault in a planetary gearbox can be determined by processing the fault signal and obtaining Its signal entropy; subsequently, its fault status can be determined based on the fault size–entropy curve that has been obtained.

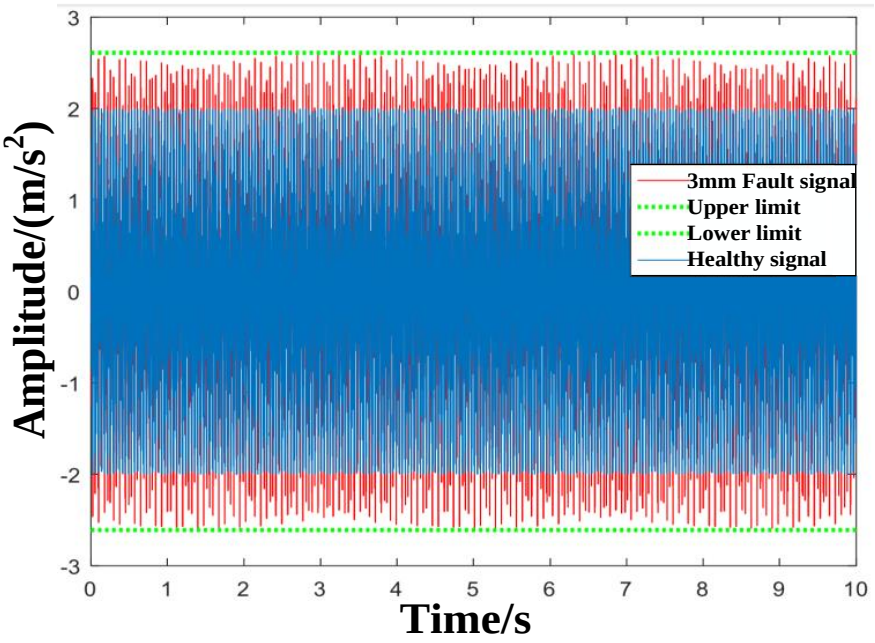

Figure 7. Boundary curves of planetary gearbox healthy and fault status signals.

4. Experimental Signal Analysis of Sun Gear Faults in Planetary Gearboxes

To verify the effectiveness of the proposed method, this work conducted tests and analysis on experimental signals of different fault sizes for the sun gear in a power transmission diagnostic test rig (Spectra GA Quest, Richmond, VA, USA), as shown in Figure 8.

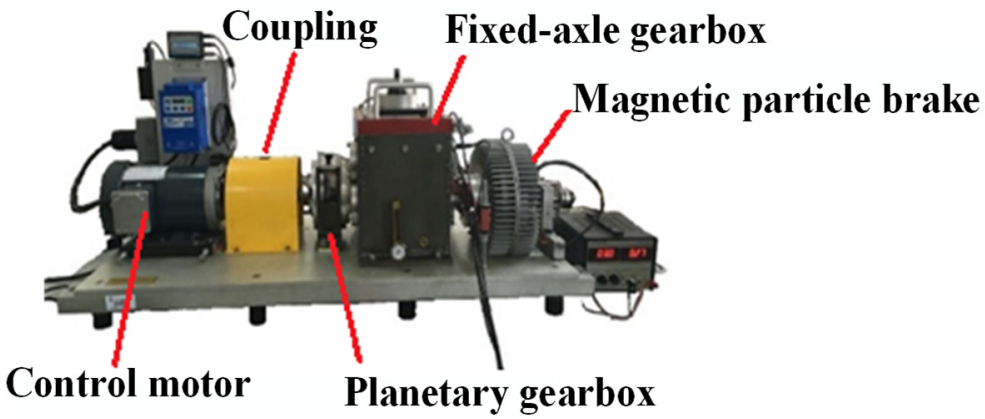

Figure 8. Power transmission fault diagnosis comprehensive test bench.

For the sake of generalization, the signals of different degrees of broken teeth and cracks in the sun gear of the planetary gearbox were analyzed. The experimental parameters of the test rig are listed in Table 2.

Table 2. Parameters of the test rig used to generate signals with different failure degrees of planetary and sun gears.

Type	Date
Sampling frequency/F_s	20,000 Hz
Maximum input shaft speed/n_s	1800 r/min
Maximum engagement frequency/f_m	600 Hz
Sun gear failure characteristic frequency/f_s	25.4 Hz
Sampling time/t	10 s
The number of teeth of the sun gear	20
The number of teeth of the planetary gears	40
The number of teeth of the geared ring	100
The number of planetary gears	3

(1) The experimental signals were variable-speed signals. To avoid the frequency ambiguity caused by traditional fault feature frequency extraction methods, the turn domain resampling method [31] was applied first to equivalently extract the signals of each group.

(2) To obtain the optimal parameter combination of K and α in the VMD transformation for each type of sun gear fault, the grid search algorithm was employed to calculate the MPE under different parameter states. The MPE values obtained under different parameter combinations for the VMD transformation of the two types of sun gear faults are exhibited in Figure 9. It can be observed that, as regards the sun gear crack fault, the optimal VMD parameter combination was K = 5 and α = 1200, while for the sun gear broken tooth fault, the optimal VMD parameter combination was K = 4 and α = 1500.

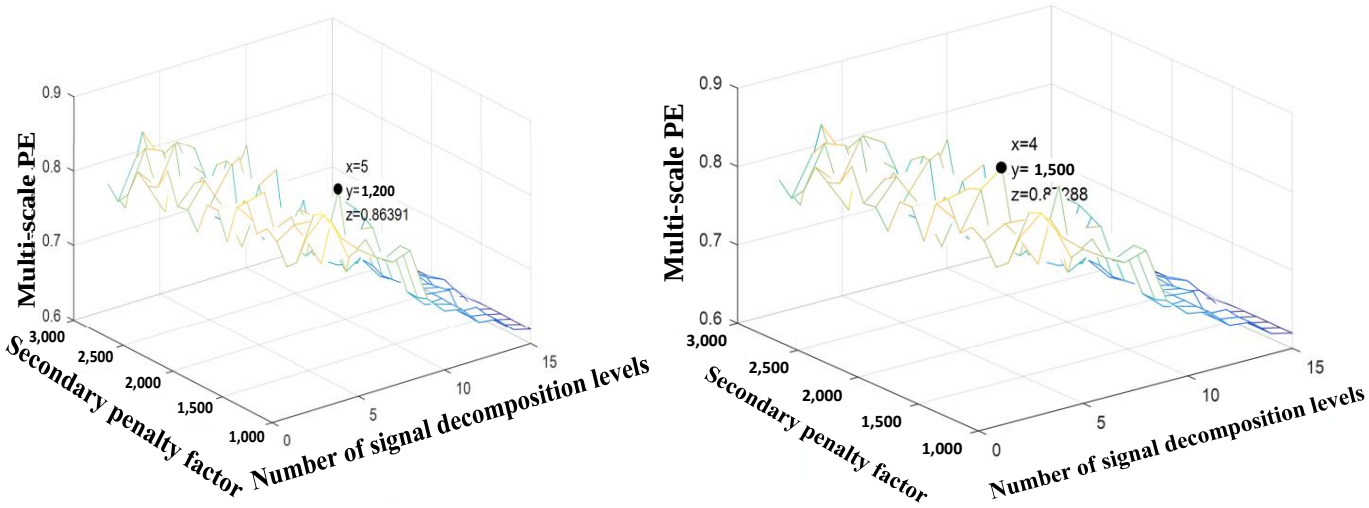

Figure 9. MPE values of VMD transformation of different parameter combinations of a sun gear with two fault conditions. (**a**) Sun gear crack failure. (**b**) Sun gear broken tooth failure.

Subsequently, the optimal parameters were used to demodulate the signals, which generated planetary gearbox fault signals with high SNR. Then, the demodulated signals were subjected to spectral analysis; the results are depicted in Figures 10 and 11. In Figures 10b and 11b, it can be seen that the spectra contained a characteristic frequency component at 25.4 Hz, which verified that the gearbox fault was a sun gear fault.

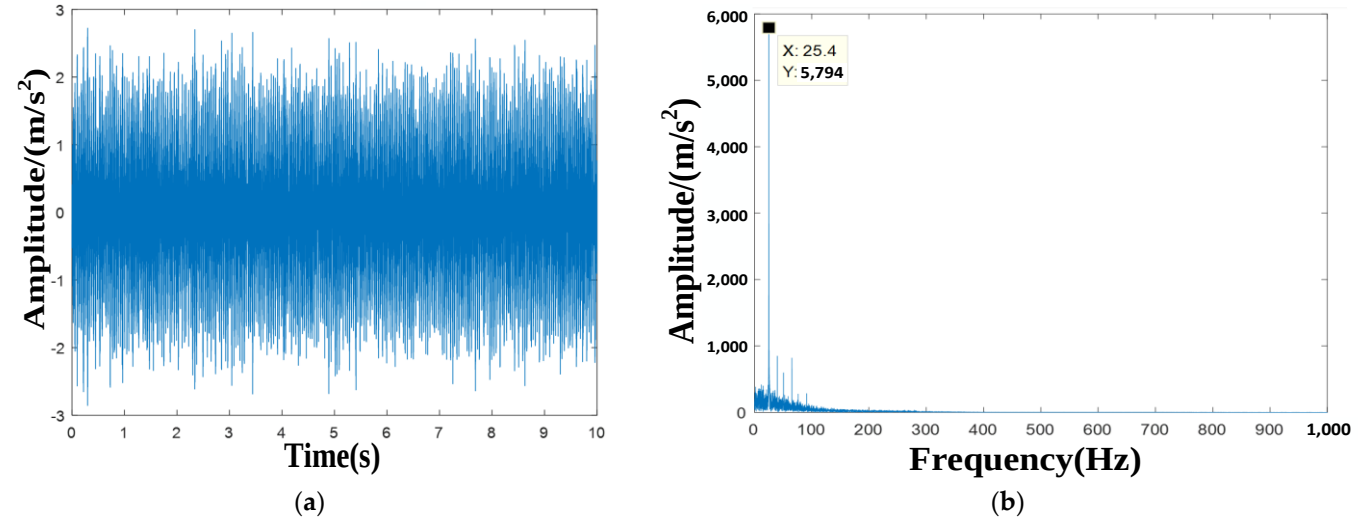

Figure 10. Time–frequency domain diagram of IVMD transformation for sun gear crack failure. (**a**) Time domain analysis of sun gear fault signal. (**b**) Frequency domain analysis of sun gear fault signal.

To reflect the advancement of the VMD method proposed in this paper, traditional VMD was used to analyze the signals of the two different types of sun gear faults; the analysis results are presented in Figures 12 and 13.

By comparing the spectra of the traditional VMD and the IVMD, it can be deduced that the denoising effect of the improved algorithm proposed in this paper was better. To further demonstrate the superiority of the proposed algorithm, the SNR of eight different sizes of sun gear crack faults was calculated.

$$SNR = 20 * ln\left(P_{signal}/P_{noice}\right) \quad (23)$$

where, P_{signal}. Is the power of the signal and P_{noise} is the power of the noise.

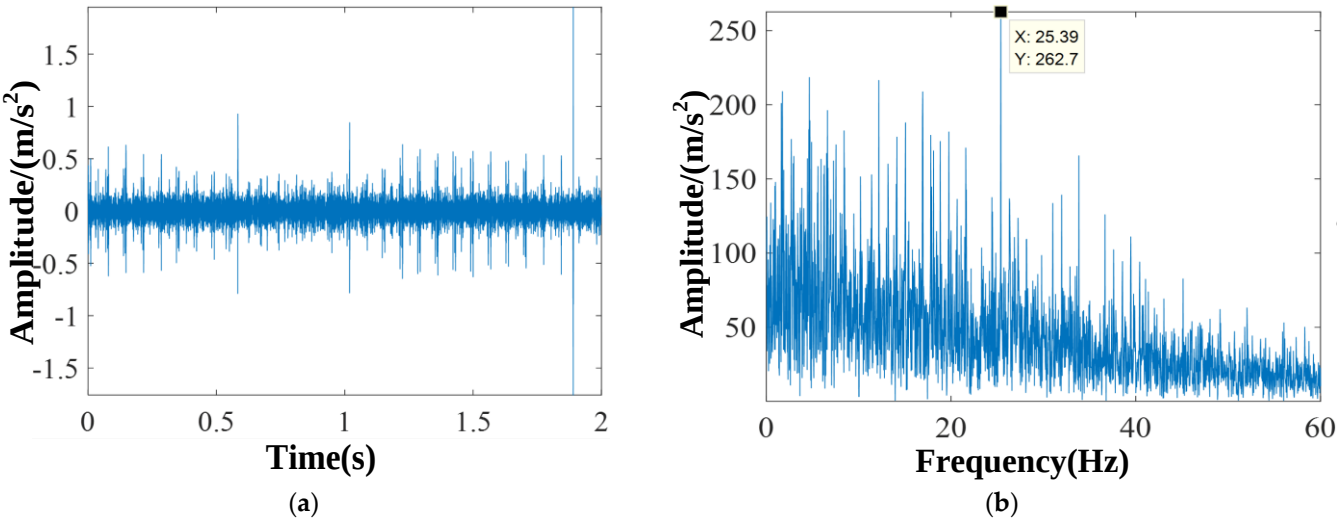

Figure 11. Time–frequency domain diagram of IVMD transformation for sun gear broken tooth fault. (**a**) Time domain analysis of sun gear fault signal. (**b**) Frequency domain analysis of sun gear fault signal.

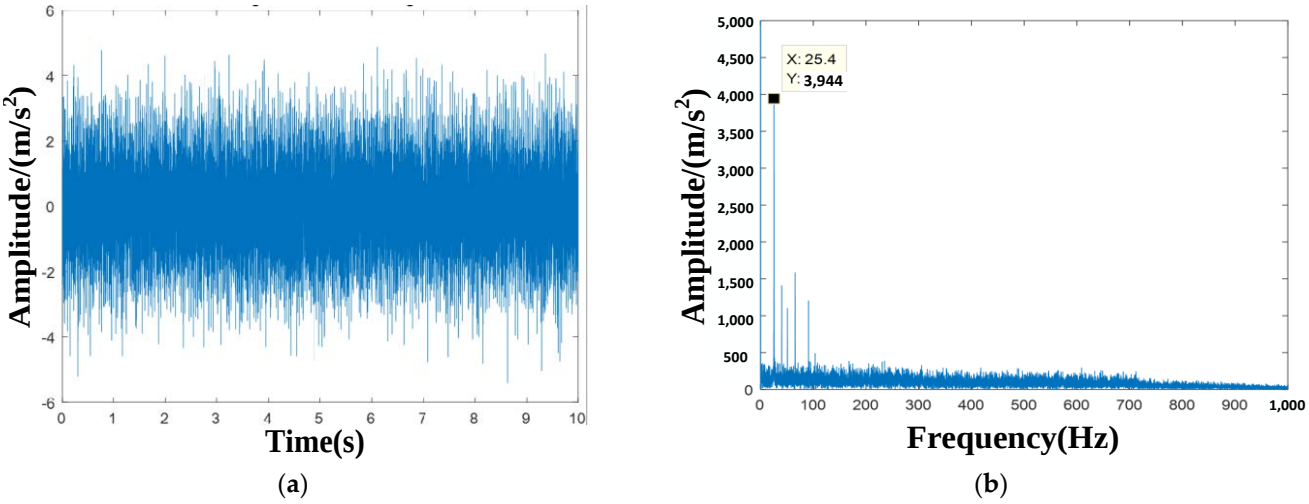

Figure 12. Traditional VMD transformation time–frequency domain diagram for sun gear crack failure. (**a**) Time domain analysis of sun gear fault signal. (**b**) Frequency domain analysis of sun gear fault signal.

Through (23), the SNR ratio responding to each fault size is obtained. The results are listed in Table 3. Compared to the traditional VMD, the SNR of IVMD was significantly improved. The above analysis proves the effectiveness of using the multi-scale permutation entropy method to optimize the VMD parameters.

(3) After improving the VMD processing, the entropy values for different fault sizes of broken teeth and cracks on the sun gear were calculated. The time domain signals after VMD processing are exhibited in Figures 14 and 15, respectively. The vibration signals of sun gear broken tooth faults of different sizes ranging from 0–7 mm are shown in Figure 13.

Table 3. SNR of traditional VMD and IVMD for sun gear crack faults with different fault sizes.

Signal Processing	IVMD	Traditional VMD
1	−1.6681	−10.1561
2	−2.7943	−9.3343
3	−1.7769	−7.4794
4	1.2260	−5.2479
5	3.0663	−3.0609
6	4.7450	−0.8851
7	6.1250	1.6454
8	8.3497	2.6639

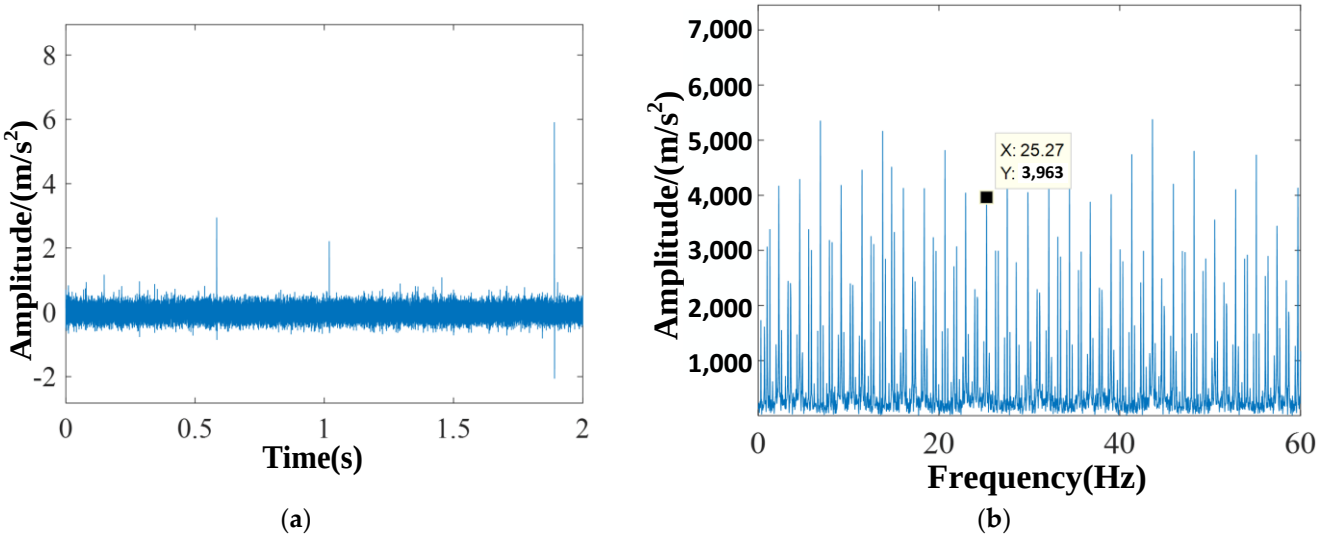

Figure 13. Traditional VMD transformation time–frequency domain diagram for sun gear broken tooth fault. (**a**) Time domain analysis of sun gear fault signal. (**b**) Frequency domain analysis of sun gear fault signal.

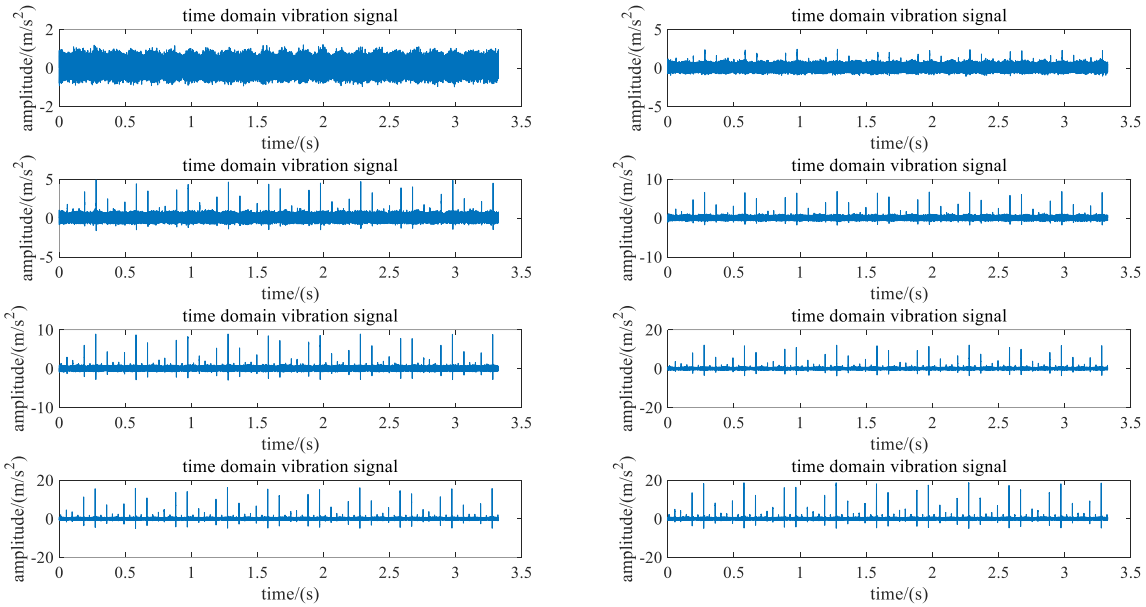

Figure 14. Time domain signals of sun gear broken teeth with different fault sizes.

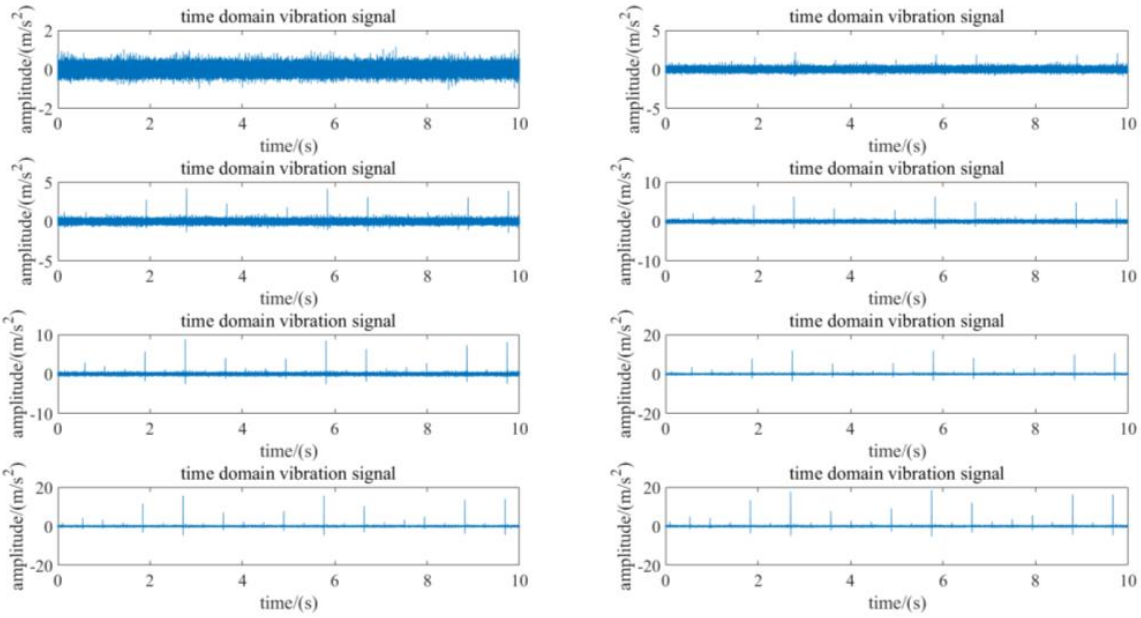

Figure 15. Time domain signal of a cracked sun gear with different fault sizes.

The failure thresholds of the sun gear faults were obtained by applying the 3-sigma principle to obtain the key characteristics of the signals, and to provide data support when performing AMDSDE parameters on subsequent signals. The results are presented in Figures 16 and 17.

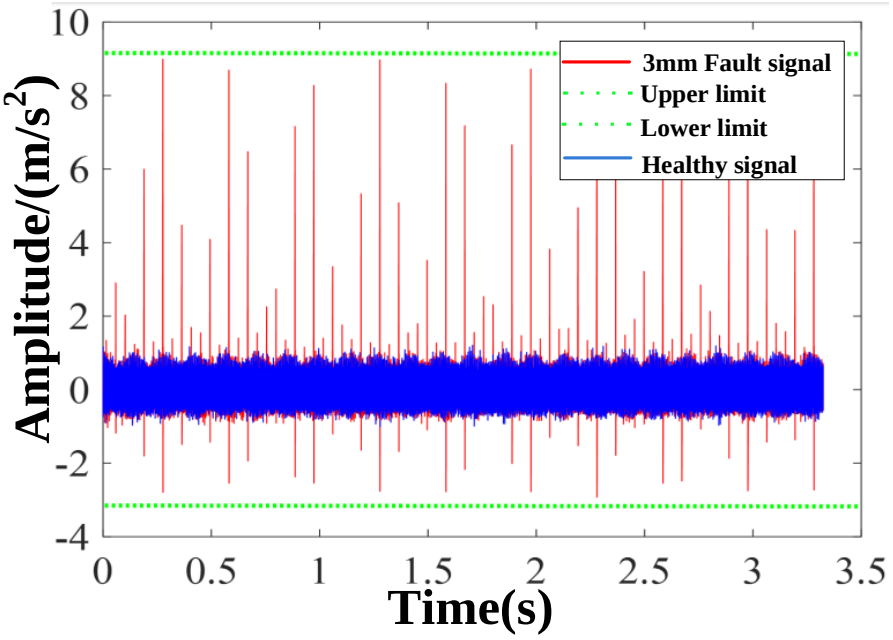

Figure 16. Failure threshold of sun gear broken tooth failure.

The AMDSDE algorithm proposed in this paper was used to calculate the entropy values of each fault size within the failure threshold range for both types of faults. The entropy variation curves were plotted and fitted using the least squares method to obtain the fault size–entropy curves. The fault size–entropy curves for sun gear broken tooth faults and crack faults are demonstrated in Figures 18 and 19, respectively.

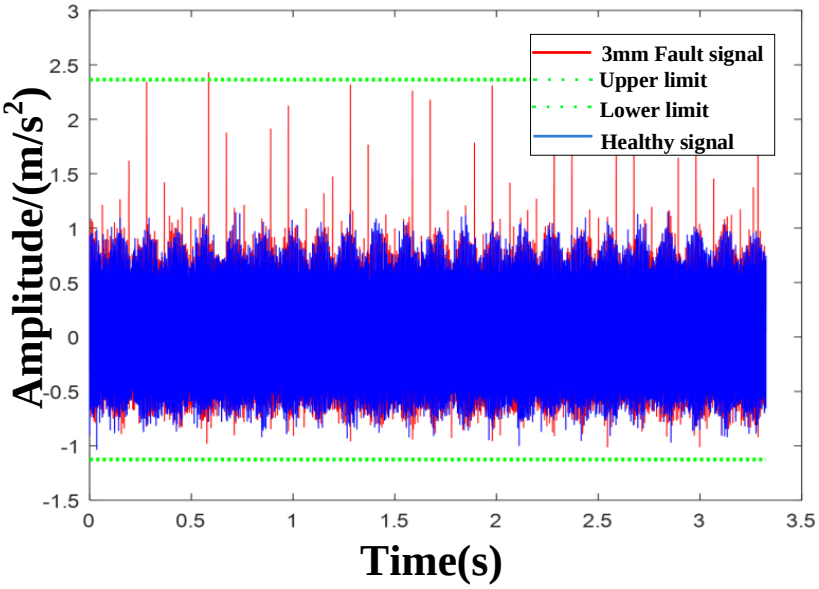

Figure 17. Failure threshold of sun gear crack failure.

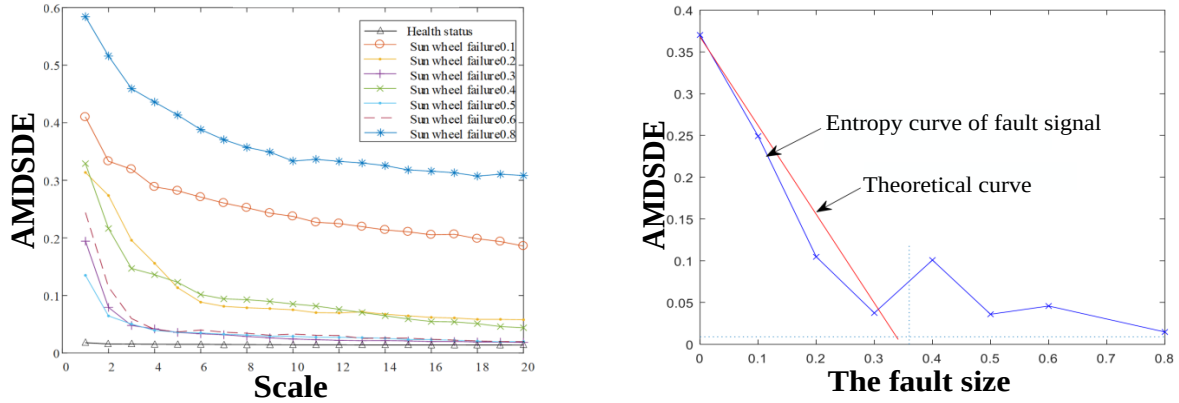

(**a**) (**b**)

Figure 18. Sun gear broken tooth fault size based on the AMDSDM curve and the dynamic entropy change curve. (**a**) Comparison curve in different sizes of healthy states. (**b**) Comparison diagram of the AMDSDE curve and the theoretical curve.

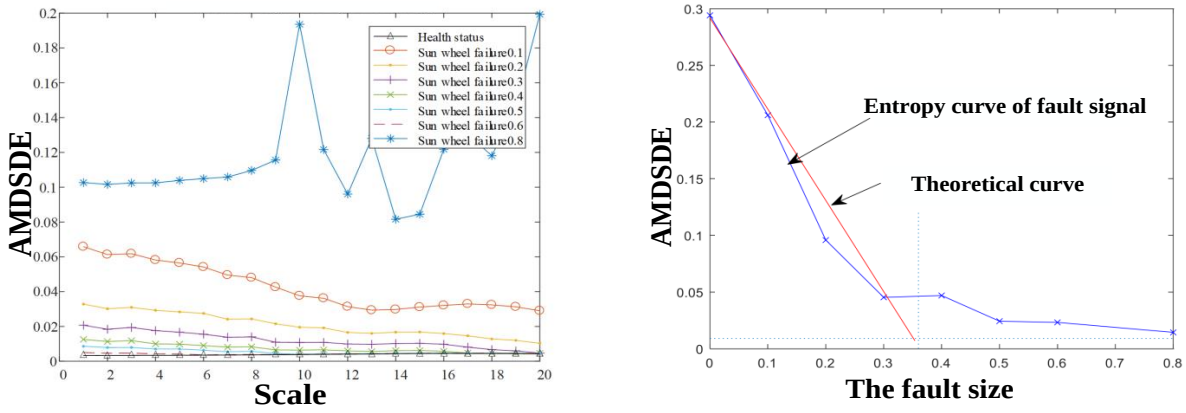

(**a**) (**b**)

Figure 19. Sun gear crack fault size and dynamic entropy change curve. (**a**) Comparison curve of AMDSDE with different sizes. (**b**) Comparison diagram of AMDSDE curve and theoretical curve.

Symbol entropy is an effective indicator that reflects the energy of periodic signals. The average dual-position symbol dynamic entropy is based on the traditional symbol entropy and includes signals from different transmission paths of the planetary gearbox. Therefore, it can effectively reflect the key components of the planetary gearbox. The fault characteristic information can be obtained to obtain a fault characteristic curve with good linearity that reflects the fault size.

In Figures 18 and 19, it can be observed that in the early fault stages, the entropy value of the sign dynamics increased approximately linearly with increasing fault size. This is because, when the fault size is small, the effect of meshing impacts on the vibration signals of the gearbox gradually weakens, and the fault impacts change almost linearly with the fault size. As the fault size increases gradually, the main impact reflected in the vibration signal is the fault impact, while the impact of other factors becomes negligible. Therefore, the entropy resembles an almost horizontal line. Based on the healthy status signals and the 3-sigma principle, the failure size of the broken teeth on the sun gear was determined to be 3.4 mm. Consequently, it can be concluded that in the early stages of sun gear broken teeth and crack faults, the fault size–entropy curves are linear, indicating that the AMDSDE index can be used to infer the corresponding fault size. The analysis of signals of sun gear broken teeth and crack faults confirms the effectiveness of the method proposed in this paper.

5. Conclusions

The paper has proposed a planetary gearbox fault diagnosis method based on IVMD transformation and AMDSDE, which can perform quantitative diagnosis of the key components in the planetary gearboxes of wind turbines. demonstrating both theoretical and practical value. The specific conclusions are drawn as follows:

(1) Combining the unique periodic characteristics and multi-scale permutation entropy of the planetary gearbox signal of the wind turbine, an IVMD algorithm based on MPE is proposed. A grid search algorithm has been used to select the combination of the decomposition layer k with the largest MPE and the quadratic penalty factor α as the optimal parameter combination for VMD transformation. This algorithm improves the SNR of the signal and is able to separate the fault impact signal from the planetary gearbox vibration signal.

(2) This paper proposes a method for fault mode recognition of key components of planetary gearboxes based on AMDSDE. The paper fully considers the impact of multiple transmission paths of planetary gearbox signals on fault impact. When calculating symbolic entropy, the entropy value under the influence of the combination of state mode probability and state transition probability obtained by adjacent modes is calculated separately, so that the calculation results eliminate the influence of amplitude difference and phase difference on fault characteristics.

(3) This study uses the proposed IVMD and AMDSDE algorithms to analyze the broken teeth and crack signals of sun gears with different fault sizes, and it obtains a fault size–entropy curve with good linearity, thus achieving quantitative diagnosis of the fault size of the planetary gearbox of the wind turbine. The experimental results show the correctness and feasibility of this method.

This algorithm improves the operating efficiency of wind turbines and reduces economic losses and personnel losses. It is currently being used in wind turbines. In the future, other equipment systems including planetary gearbox structures will be promoted and further research will be conducted. Future research should focus on predicting the remaining life of planetary gearboxes through AMDSDE.

Author Contributions: Conceptualization, Y.W., J.M. and T.L.; methodology, T.L.; soft-ware, T.L.; validation, Y.W.; formal analysis, T.L.; investigation, J.M.; resources, T.L.; data curation, T.L.; writing—original draft preparation, T.L. and C.Z.; writing—review and editing, J.M.; supervision, J.M.; project administration, T.L.; funding acquisition, J.M. and C.Z. All authors have read and agreed to the published version of the manuscript.

Funding: This study was funded by the National Natural Science Foundation of China (No. 51965052), the National Natural Science Foundation of China (No. 52365014) and the Science and Technology Planning Project of Inner Mongolia Autonomous Region (No. 2022YFHH0122), the Technology Planning Project of Inner Mongolia Autonomous Region (No. 2023YFSW0003) and the Natural Science Foundation of Inner Mongolia (No. 2023QN05031).

Data Availability Statement: Because the data involved in this paper need to be further studied, they will not be disclosed here.

Acknowledgments: The authors would like to gratefully acknowledge the National Natural Science Foundation of China and the Science and Technology Planning Project of Inner Mongolia Autonomous Region and the Inner Mongolia Key Laboratory of Intelligent Diagnosis and Control of Mechatronic Systems. Finally, the authors would like to thank the editors and reviewers for their valuable comments and constructive suggestions.

Conflicts of Interest: The authors declare no conflicts of interest.

References

1. Dou, C.H. Fault Feature Extraction for Gearboxes Using Empirical Mode Decomposition. *Adv. Mater. Res.* **2012**, *383–390*, 1376–1380. [CrossRef]
2. Huang, J.; Cui, L. Tensor Singular Spectrum Decomposition: Multisensor Denoising Algorithm and Application. *IEEE Trans. Instrum. Meas.* **2023**, *72*, 3510015. [CrossRef]
3. Xu, H.; Wang, X.; Huang, J.; Chu, F. Semi-supervised multi-sensor information fusion tailored graph embedded low-rank tensor learning machine under extremely low labeled rate. *Inf. Fusion* **2024**, *105*, 102222. [CrossRef]
4. Huang, J.; Zhang, F.; Babak, S.; Qin, Z.; Chu, F. The flexible tensor singular value decomposition and its applications in multisensor signal fusion processing. *Mech. Syst. Signal Process.* **2024**, *220*, 111662. [CrossRef]
5. Yang, P.; Li, C.; Bin, G.; Miao, H.; Gu, F. Erosion wear patterns of turboshaft engine compressor under different radial inlet distortion conditions. *Tribol. Int.* **2024**, *198*, 109907. [CrossRef]
6. Zhang, Y.; Yu, K.; Lei, Z.; Ge, J.; Xu, Y.; Li, Z.; Ren, Z.; Feng, K. Integrated intelligent fault diagnosis approach of offshore wind turbine bearing based on information stream fusion and semi-supervised learning. *Expert Syst. Appl.* **2023**, *232*, 120854. [CrossRef]
7. Zhang, Y.; Ji, J.; Ren, Z.; Ni, Q.; Gu, F.; Feng, K.; Yu, K.; Ge, J.; Lei, Z.; Liu, Z. Digital twin-driven partial domain adaptation network for intelligent fault diagnosis of rolling bearing. *Reliab. Eng. Syst. Saf.* **2023**, *234*, 109186. [CrossRef]
8. Zhang, Y.; Ren, Z.; Feng, K.; Yu, K.; Beer, M.; Liu, Z. Universal source-free domain adaptation method for cross-domain fault diagnosis of machines. *Mech. Syst. Signal Process.* **2023**, *191*. [CrossRef]
9. Dragomiretskiy, K.; Zosso, D. Variational Mode Decomposition. *IEEE Trans. Signal Process.* **2014**, *62*, 531–544. [CrossRef]
10. Soltani, B.I. A Combined Spectral Subtraction and Wavelet De-Noising Method for Bearing Fault Diagnosis. In Proceedings of the 2007 American Control Conference, New York, NY, USA, 9–13 July 2007.
11. Upadhyay, A.; Pachori, R. Speech enhancement based on mEMD-VMD method. *Electron. Lett.* **2017**, *53*, 502–504. [CrossRef]
12. Isham, M.F.; Leong, M.S.; Lim, M.H.; Zakaria, M.K. A review on variational mode decomposition for rotating machinery diagnosis. In *MATEC Web of Conferences*; EDP Sciences: Les Ulis, France, 2019; Volume 255. [CrossRef]
13. Gilt, G. An ECG Signal Denoising based on VMD and Undecimated Wavelet Transform. *Int. J. Sci. Res. Dev.* **2016**, *4*, 1029–1033.
14. Li, F.; Li, R.; Tian, L.; Chen, L.; Liu, J. Data-driven time-frequency analysis method based on variational mode decomposition and its application to gear fault diagnosis in variable working conditions. *Mech. Syst. Signal Process.* **2018**, *116*, 462–479. [CrossRef]
15. Zheng, Y.; Yue, J.H.; Jiao, J.; Guo, X.Y. Fault feature extraction method of rolling bearing based on parameter optimized VMD. *J. Vib. Shock.* **2021**, *40*, 86–94.
16. Tang, D.; Bi, F.; Lin, J.; Li, X.; Yang, X.; Bi, X. Adaptive Recursive Variational Mode Decomposition for Multiple Engine Faults Detection. *IEEE Trans. Instrum. Meas.* **2022**, *71*, 3513111. [CrossRef]
17. Li, K.; Niu, Y.Y.; Su, L. Rolling bearing fault diagnosis method based on parameter optimized VMD. *J. Vib. Eng.* **2023**, *36*, 280–287.
18. Shannon, C.E. A mathematical theory of communication. *ACM SIGMOBILE Mob. Comput. Commun. Rev.* **2001**, *5*, 3–55. [CrossRef]
19. Noman, K.; He, Q.; Peng, Z.-K.; Wang, D. A scale independent flexible bearing health monitoring index based on time frequency manifold energy & entropy. *Meas. Sci. Technol.* **2020**, *31*, 114003. [CrossRef]
20. Shen, Y.J.; Wang, J.F.; Yang, S.P. Improved method for detecting weak abrupt information based on permutation entropy. *Adv. Mech. Eng.* **2019**, *9*, 1–9. [CrossRef]
21. Wang, S.; Li, Y.; Si, S.; Noman, K. Enhanced hierarchical symbolic sample entropy: Efficient tool for fault diagnosis of rotating machinery. *Struct. Health Monit.* **2022**, *22*, 1927–1940. [CrossRef]
22. Zheng, J.; Chen, Y.; Pan, H.; Tong, J. Composite multi-scale phase reverse permutation entropy and its application to fault diagnosis of rolling bearing. *Nonlinear Dyn.* **2023**, *111*, 459–479. [CrossRef]
23. Deka, B.; Deka, D. An improved multiscale distribution entropy for analyzing complexity of real-world signals. *Chaos Solitons Fractals* **2022**, *158*, 112101. [CrossRef]

24. Daw, C.S.; Finney, C.E.A.; Tracy, E.R. A review of symbolic analysis of experimental data. *Rev. Sci. Instrum.* **2003**, *74*, 915–930. [CrossRef]
25. Kurths, J.; Voss, A.; Saparin, P.; Witt, A.; Kleiner, H.J.; Wessel, N. Quantitative analysis of heart rate variability. *Chao* **1995**, *5*, 88–94. [CrossRef] [PubMed]
26. Chen, F.; Wang, B.; Zhou, D.; Zhao, Z.; Ding, C.; Chen, D. A fault diagnosis method for shaft system of hydropower units based on improved symbolic dynamic entropy and stochastic configuration network. *J. Hydraul. Eng.* **2022**, *53*, 1127–1139.
27. Costa, M.; Goldberger, A.; Peng, C. Multiscale entropy to distinguish physiologic and synthetic RR time series. *Comput. Cardiol.* **2002**, *29*, 137–140. [CrossRef]
28. Ding, C.; Feng, F.; Zhang, B.; Wu, S. MMSDE and its application in feature extraction of a planetary gearbox. *J. Vib. Shock.* **2020**, *39*, 97–102.
29. Li, Y.; Yang, Y.; Li, G.; Xu, M.; Huang, W. A fault diagnosis scheme for planetary gearboxes using modified multi-scale symbolic dynamic entropy and mRMR feature selection. *Mech. Syst. Signal Process.* **2017**, *91*, 295–312. [CrossRef]
30. Han, M.; Wu, Y.; Wang, Y.; Liu, W. Roller bearing fault diagnosis based on LMD and multi-scale symbolic dynamic information entropy. *J. Mech. Sci. Technol.* **2021**, *35*, 1993–2005. [CrossRef]
31. Liu, T.; Cui, L.; Zhang, C. Study on Fault Diagnosis Method of Planetary Gearbox Based on Turn Domain Resampling and Variable Multi-Scale Morphological Filtering. *Symmetry* **2020**, *13*, 52. [CrossRef]